JMEPEG
https://doi.org/10.1007/s11665-023-09032-8

1059-9495/$19.00

ORIGINAL RESEARCH ARTICLE

Effect of CeO_2 Addition on Microstructure, Hardness, and Tensile Properties of Selected Laser-Melted TC4 Alloys

Zhenhua Li, Yu Zhang, Bo Yin, and Dudu Song

Submitted: 4 August 2023 / Revised: 15 November 2023 / Accepted: 25 November 2023

The effects of CeO_2 content on microstructure and mechanical properties of TC4 titanium alloy samples produced by selective laser melting were investigated using optical microscopy, scanning electron microscopy, x-ray diffraction, and microhardness and mechanical tensile testing. In the absence of CeO_2, microstructures of the TC4 samples produced by selective laser melting mainly consisted of Widmanstätten α plates, a small amount of needle-like α′ phase, and some β phases, and exhibited high strength and low plasticity. On adding a small amount (0.1%) of CeO_2, grains within the structure became more refined, as the Widmanstätten α plates started to transform into a basket-weave structure: strength and plasticity were improved. When the CeO_2 addition was 0.15%, the yield and tensile strengths of the samples were, respectively, increased by 39.5% and 17.5% compared with the values of the rare-earth-free alloy. With an increase in CeO_2 content to 0.2%, the microstructure began to coarsen, strength and plasticity decreased, and hardness increased. When the CeO_2 content reached 1%, the alloy hardness was 398 HV, but its fragility became severe. CeO_2 refined the grain size of the sample structures by inhibition of solute growth and reduced unfused defects in the TC4 powder, ultimately improving the alloy strength.

Keywords mechanical properties, microstructure, rare earth, selective laser melting, TC4 titanium alloy

1. Introduction

Ti-6Al-4V (TC4) is a dual-phase titanium alloy that combines the advantages of both α and β phases, making it widely used in aerospace and marine engineering fields due to its good tissue stability, plasticity, toughness, and high-temperature deformation properties (Ref 1-3). Selective laser melting (SLM) can be utilized for integrated and controlled forming of highly complex titanium alloy components, effectively solving the challenges of high energy consumption, long production cycles, low material utilization, and difficulty in forming complex titanium alloy parts (Ref 4, 5). However, during preparation using SLM, rapid heating and transient condensation of the melt pool cause the metallic material to experience repeated thermal expansion and contraction, triggering thermal and phase-change stresses (Ref 6, 7). Coupled with the existence of interstitial debris, qualitative elements (such as O, S), and defects in the powder itself, such as porosity in the titanium alloy powder (Ref 8-11), it is difficult to avoid the presence of unmelted powder and other metallurgical defects during the forming process. These phenomena affect the forming quality, density, and mechanical properties of titanium alloys to varying degrees.

In recent years, there has been widespread attention to improving the forming quality of additive-manufacturing alloys by doping them with rare-earth elements. The addition of trace amounts of rare-earth elements can effectively enhance the mechanical properties of titanium alloys. Rare-earth elements can combine with oxygen or other alloying elements to form highly stable second-phase particles at high temperatures (Ref 12, 13), which have the ability to refine the β-Ti grains. Yang et al. (Ref 14) found that adding a small amount of $CeSi_2$ to TC4 alloy can remove oxygen (O) and chlorine (Cl) from Ti powder, thereby improving ductility of the alloy. The resulting CeO_2 and $CeCl_xO_y$ particles produce a pinning effect at the grain boundaries, which limits the growth of β grains and refines the α-Ti platelets. Li et al. (Ref 15) improved the mechanical properties of as-cast TC4 alloy by adding 0.1 mass% Ce, which increased the tensile strength of the cast TC4 alloy from 787 to 957 MPa and the elongation from 8.8 to 12.3%. Analysis revealed that Ce can absorb harmful elements from the lattice during the alloy-solidification process, by forming uniformly distributed compounds. These compounds introduce more nucleation sites for the cast alloy, refine the β-phase lamellar structure, and further improve alloy strength. Xu et al. (Ref 16) prepared TC4 alloys with a small amount of Ce using a vacuum non-consumable arc furnace. The tensile strength and ductility of a TC4 sample containing 0.5 mass% Ce were significantly improved, which was attributed to the refinement effect of cerium oxide nanoparticles formed in the alloy and the coherent relationship between these nanoparticles and the TC4 matrix.

There is currently limited research on the effect on the properties of SLM-formed TC4 alloy of adding trace amounts

Zhenhua Li, Yu Zhang, Bo Yin, and **Dudu Song**, Marine Engineering Equipment College, Zhejiang Ocean University, Zhoushan 316022 Zhejiang, China. Contact e-mail: lizh760905@zjou.edu.cn.

Published online: 18 December 2023

of CeO_2. This study aimed to investigate the influence of CeO_2 content on the microstructure and mechanical properties of SLM-formed TC4 alloys, thereby providing valuable insights for improving SLM-formed defects and optimizing the strength–ductility match of SLM-formed titanium alloys. In addition to its low cost, CeO_2 has the following advantages: firstly, it is itself a high-temperature stable second-phase particle, and can increase fluidity of the melt pool, reduce defects in the formed melt track, and decrease crack formation. Wang et al. (Ref 17) found that adding CeO_2 to a Ni60 alloy surface laser cladding on aluminum alloy improved the fluidity of the melt pool, enhanced wetting between the cladding layer and substrate, and facilitated escape of gases from the metal melt, thereby reducing defects such as bubbles and cracks in the Ni60 alloy surface. Secondly, under high-energy irradiation from a laser, CeO_2 will partially or completely decompose into Ce and O_2, the latter of which will then recombine with oxygen in the liquid metal to form CeO_2 and Ce_2O_3. These stable oxide particles become pinned at grain boundaries and phase boundaries, hindering grain growth and achieving refinement. They can also impede dislocation movement in the alloy microstructure and improve alloy strength. When combined with SLM, which is an effective rapid-solidification processing method, rare-earth elements are able to achieve high solubility in titanium alloys due to extremely fast cooling rates. Such a non-equilibrium supersaturated solid solution will decompose and form small uniform rare-earth second-phase particles at certain temperatures (Ref 18-20).

2. Materials and Methods

TC4 titanium alloy spherical powder with a particle size of 15-53 μm and chemical composition shown in Table 1, produced by AVIMETAL MET Powder Metallurgy Technology Co., Ltd. (China), was employed. The rare-earth powder used was CeO_2 powder with an average particle size of 50 nm, produced by Anhui Xuancheng Jingrui New Materials Co., Ltd. (China). Figure 1(a) and (b) shows particle morphologies of the TC4 titanium alloy and CeO_2 powders, respectively. Prior to printing, the TC4 titanium alloy and CeO_2 powders were evenly mixed in a mixer (total mixing time of 500 min, with a pause of 10 s every 10 min to reverse rotation). Figure 1(c) shows the TC4 powder with a CeO_2 mass fraction of 0.15%. The powders were subsequently vacuum dried at 110 °C for 2 h.

The SLM equipment was model number EP-M150, manufactured by Beijing e Plus 3D Tech Co., Ltd. (China). Argon (purity: 99.99%) was used as the protective gas. The substrate material formed was TA1. To ensure the quality of the formed parts, the laser power and scanning speed should be set within reasonable ranges. Experiments conducted by Wang and Sun (Ref 21, 22) showed that the optimal comprehensive effect on the forming quality of TC4 alloy by SLM is achieved when the laser power is set at 175-250 W and the scanning speed is 850-1150 m/s^{-1}. Considering the limitations of the equipment, the main forming technical parameters were as follows: laser power of 180 W, scanning speed of 1000 mm/s, and layer thickness of 40 μm.

After etching with Kroll reagent, the formed specimens were observed under an optical microscope (OM; BM-12A) and scanning electron microscope (SEM; Zeiss Sigma500) to analyze the influence of CeO_2 on the microstructure of SLM-formed TC4. Phase composition of the samples was analyzed using a MiniFlex6 x-ray diffractometer. The microhardness and tensile properties of the specimens were tested using a VH3300 Vickers hardness tester and Zwick Z100 universal testing machine, respectively. A schematic diagram of the sample-stretching process used to manufacture the tensile testing samples is shown in Fig. 2. The equipment uniformly spread the powder from the powder cylinder onto the forming cylinder using a recoater blade to create a predetermined layer thickness. The laser beam focused on the surface of the powder bed through a scanning mirror and melted the powder according to the model slicing path. The stretching sample was built up in a layer-by-layer manner.

3. Results and Discussion

3.1 Microstructure Characteristics

Figure 3 and 4 show the crystal phase organization of the TC4 titanium alloy samples prepared by SLM by OM and SEM, respectively. Figure 3(a) shows that the original TC4 sample mainly comprised coarse and elongated columnar crystals with a width of 125-150 μm, which is similar to the observations of Zhang and Kaschel (Ref 23, 24). The SEM image in Fig. 4(a) shows that the original columnar β-Ti crystal structure consisted mainly of Widmanstätten α plates, needle-like α' phase, and certain volume fractions of β phase. A high cooling rate can refine the alloy structure (Ref 25), while the needle-like α' phase mainly originated from transformation of β phase under rapid cooling conditions.

As shown in Fig. 4(b), on adding 0.1% CeO_2, the grain width slightly decreased, the original Widmanstätten α plates decreased, and there was some fragmentation around the α and β phases, producing a rudimentary mesh-like structure. When the mass fraction of CeO_2 increased to 0.15%, the alternating dark and bright phenomena in the macroscopic microstructure became less apparent (Fig. 3b) and the grains became significantly refined. The microstructure is transformed from staggered Widmanstätten α plates to mesh-like α plates (Fig. 4c).

When the mass fraction of CeO_2 reached 0.2%, the width of the grains began to increase, the number of coarse α plates significantly increased, and small clusters of bundled structures appeared (Fig. 4d). With addition of 1% CeO_2, columnar

Table 1 Chemical composition of TC4 titanium alloy powder, mass%

Ti	Al	V	Fe	C	O	N	H
Bal.	5.50-6.50	3.50-4.50	≤ 0.25	≤ 0.08	≤ 0.20	≤ 0.05	≤ 0.012

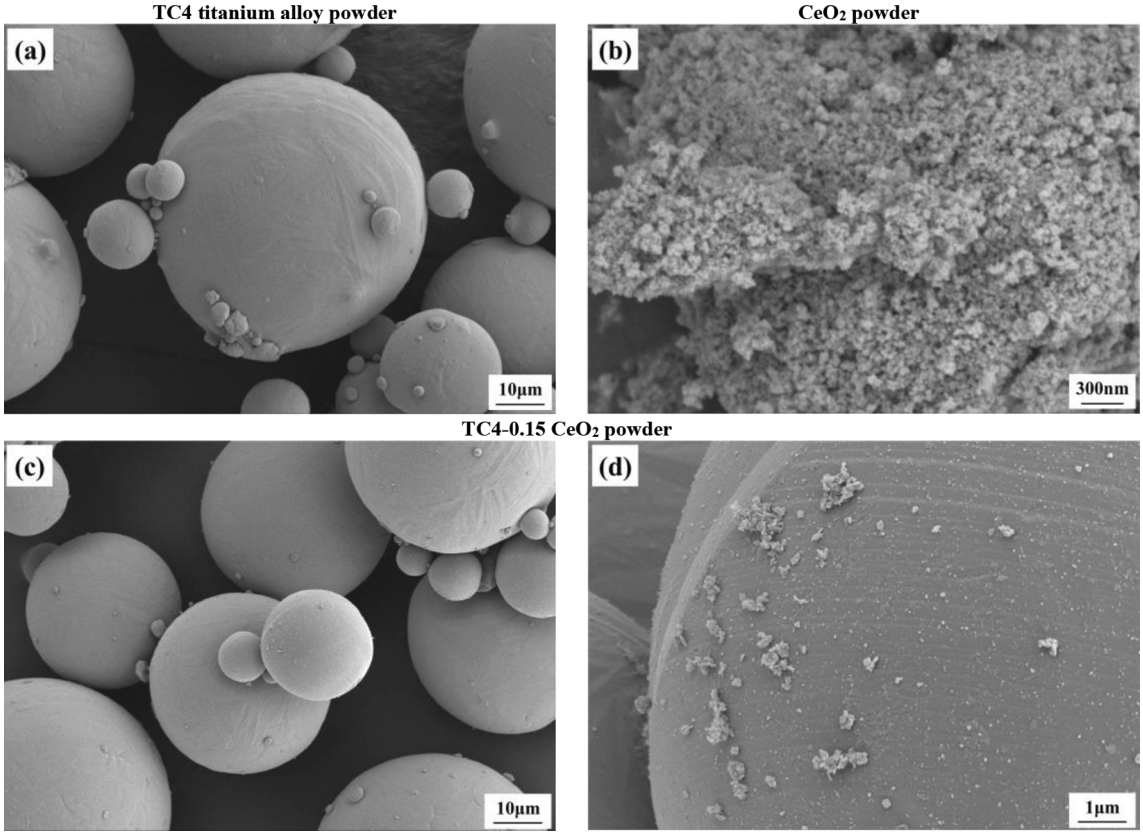

Fig. 1 Microstructures of (a) TC4 titanium alloy powder; (b) CeO_2 powder; (c) TC4-0.15 CeO_2 powder; (d) partially enlarged image of (c)

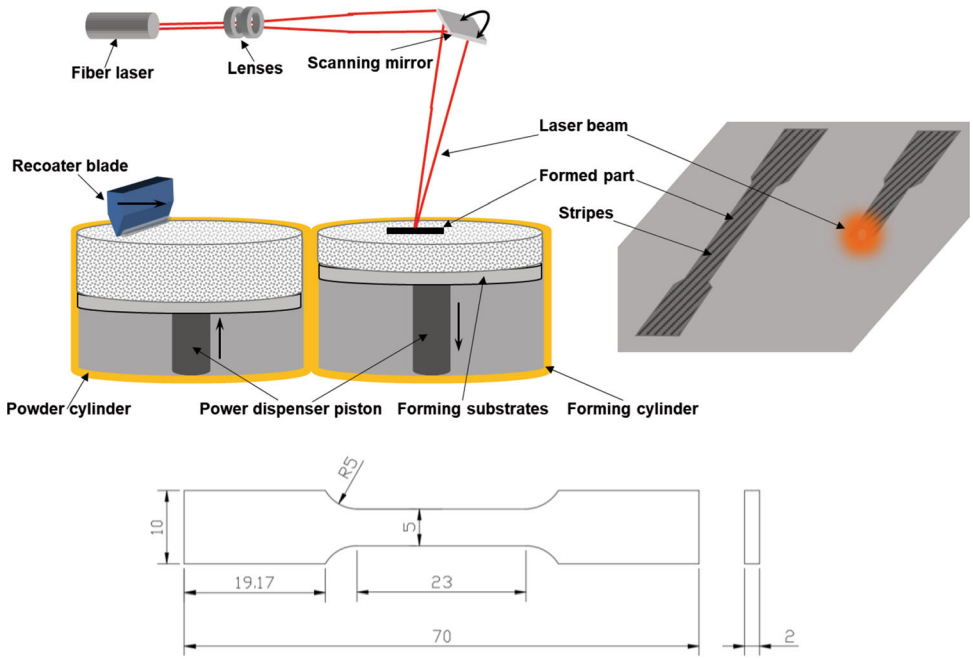

Fig. 2 Manufacture and configuration of samples used for tensile tests

crystals reappeared, exhibiting an aggregated state (Fig. 3c). The grain size further increased, with the production of lamellar α and β phases, resulting in significant coarsening of the structure (Fig. 4e). Moreover, white particles were observed on the alloy surface: the content was too low to be identified by energy-dispersive spectroscopy, but it is speculated that these were CeO_2 particles.

Table 2 shows the length and width dimensions of the α phase of SLM-formed TC4 at room temperature for different mass fractions of CeO_2. The dimensions were manually

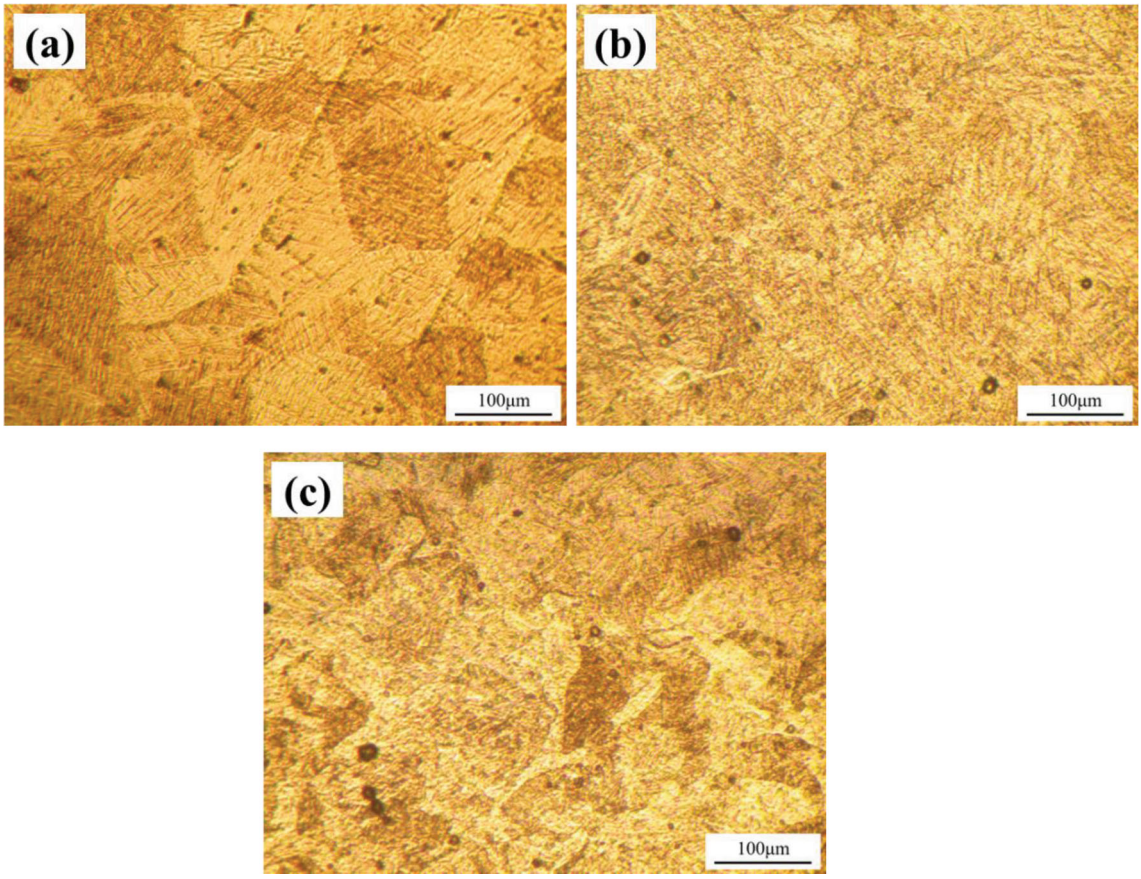

Fig. 3 Optical micrographs of microstructures of TC4-xCeO$_2$ alloy specimens: (a) pure TC4; (b) TC4-0.15CeO$_2$; (c) TC4-1CeO$_2$

measured using ImageJ image processing software, with fifty α-phase samples randomly selected for each alloy and the average value taken. Combining the data from Figure 3 and 4, it can be observed that as the amount of added CeO_2 increased, refinement of the alloy microstructure became more pronounced. TC4-0.15CeO_2 exhibited the best refinement, with the width of the α phase decreasing from 1.05 to 0.49 μm; however, when addition of CeO_2 exceeded 0.15%, the microstructure began to coarsen and the dimensions of the α phase showed an increasing trend.

3.2 Phase Composition

Figure 5 shows x-ray diffraction (XRD) patterns of SLM-formed TC4, TC4-0.15CeO_2, and TC4-1CeO_2 alloys. The SLM-formed TC4 primarily comprised α phase. This indicates that the quantity of β phase was relatively small because the diffraction peaks were easily obscured by α-phase diffraction peaks and hence not prominently displayed. CeO_2 peaks appear in the XRD spectra of the TC4-0.15CeO_2 and TC4-1CeO_2 alloys, increasing in intensity to some extent as the CeO_2 content increased. When the mass fraction of CeO_2 increased to 1%, a Ce_2O_3 peak appeared in the XRD spectra. This agrees with observations of Liu and Yang (Ref 14, 26). Comparing the diffraction peaks of the three materials, that of TC4-0.15CeO_2 was slightly shifted to the right (higher 2θ). The reason for the shift may be due to deviation of the detection system; however, the detailed graph in Figure 5 shows that the overall degree and direction of the diffraction peak shift of TC4-0.15CeO_2 are the same. Therefore, it is more likely that CeO_2 causes different degrees of lattice distortion in the α and β phases.

Bragg's diffraction equation and the formula for calculating the crystal plane distances of the α and β phases are shown in Equation 1 and 2, respectively (Ref 27, 28). These can be used to explain the shift of the diffraction peaks to the right for TC4-0.15CeO_2. In Equation 1, $d(hkl)$ is the interplanar spacing, θ is the diffraction angle, and λ is the x-ray wavelength (a constant). The right shift of the diffraction peaks for the α and β phases indicates that θ increased and d(hkl) decreased. Combined with Equation 2, where a is the lattice constant, and h, k, and l are crystal indices, it is obvious that a decrease in interplanar spacing $d(hkl)$ will cause the lattice constant to decrease. Therefore, as the diffraction peaks shift to the right, the lattice constants of the α and β phases in the alloy decrease, resulting in an increase in the number of grain boundaries and grains with different orientations within a certain volume of the crystal, which leads to grain refinement (Ref 29). This is consistent with the experimental observations of the microstructures.

$$2d(hkl)\sin\theta = \lambda \quad \text{(Eq 1)}$$

$$d(hkl) = \frac{\mathrm{a}}{\sqrt{h^2 + k^2 + l^2}} \quad \text{(Eq 2)}$$

Refinement of the organization may benefit from the growth-inhibition effect of rare-earth elements as solutes. During a solidification process, enrichment/depletion of solutes in the liquid phase at the solid–liquid interface can cause

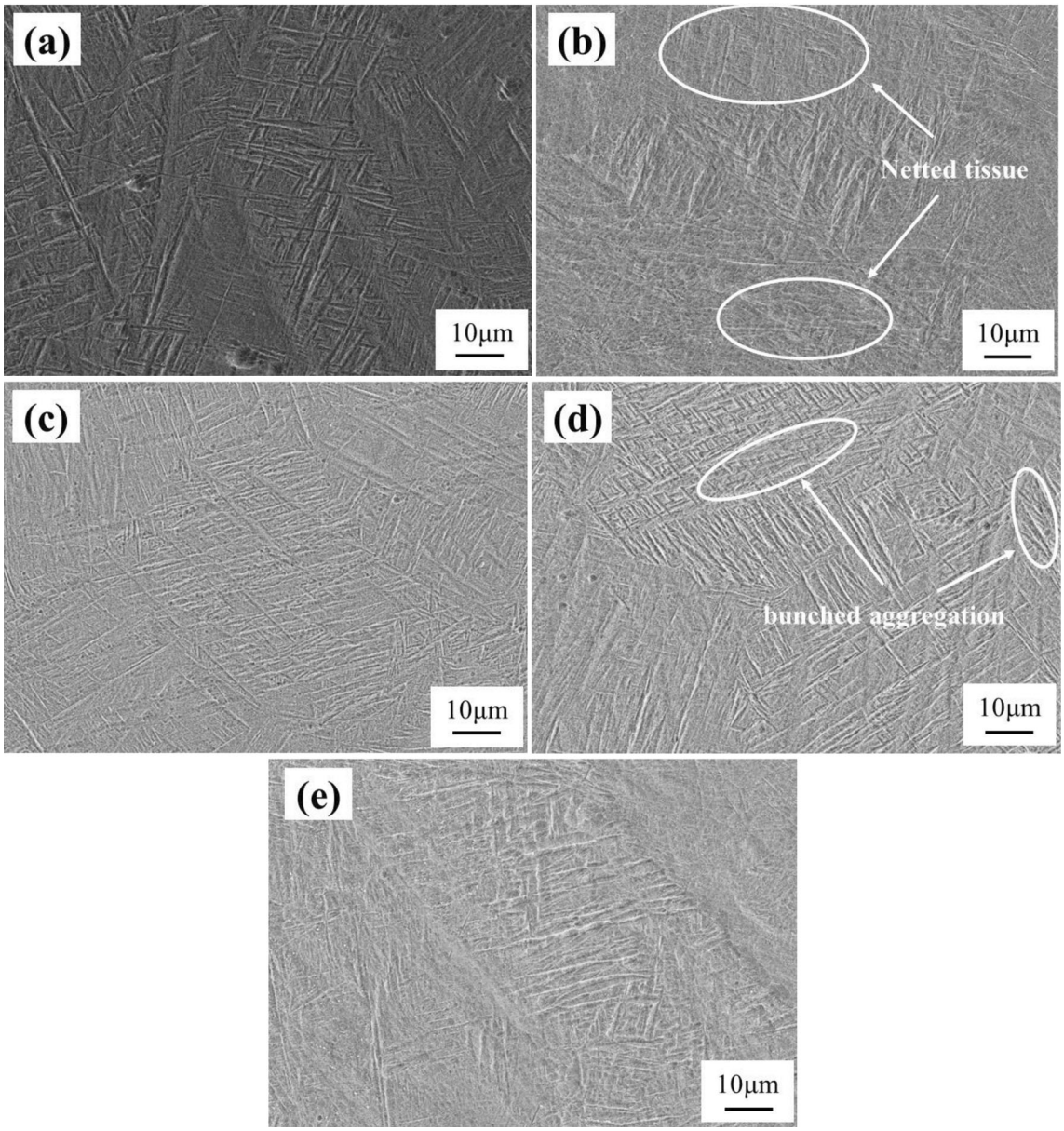

Fig. 4 Scanning electron micrographs of microstructures of TC4-xCeO$_2$ alloy specimens: (a) pure TC4; (b) TC4-0.1CeO$_2$; (c) TC4-0.15CeO$_2$; (d) TC4-0.2CeO$_2$; (e) TC4-1CeO$_2$

Table 2 Average length and average width of TC4-xCeO$_2$ sample α plates

Alloy	Length of α plates, μm	Width of α plates, μm
Pure TC4	21.45	1.05
TC4-0.1CeO$_2$	13.51	0.81
TC4-0.15CeO$_2$	7.97	0.49
TC4-0.2CeO$_2$	14.19	0.66
TC4-1CeO$_2$	16.38	1.10

undercooling, leading to formation of new nuclei in the undercooled region. This increases the nucleation rate and hinders growth of previously formed nuclei, thereby refining the grain size. Effective solutes have a high growth-restriction factor Q, which is defined as the rate of development of the undercooled region during the solidification process (Ref 29, 30) and can be calculated using Equation 3.

$$Q = mC_0(k - 1) \quad \text{(Eq 3)}$$

In the binary phase diagram, m represents the slope of the liquid-phase line (K/mass%); C_0 represents the concentration of solute elements (mass%); k is the equilibrium distribution coefficient of solute elements; Q represents the rate of formation of component undercooling caused by solute enrichment/depletion (K). The larger the Q value, the faster is the formation rate, which means that the grain size will be smaller (Ref 31-34). As shown in Table 3 (Ref 35), adding CeO$_2$ to TC4 can improve the degree of undercooling and refine the grain size.

Regarding the effect of solute growth inhibition, some researchers have drawn similar conclusions. Zhang et al. (Ref 36) proposed that the reason for tissue refinement was that

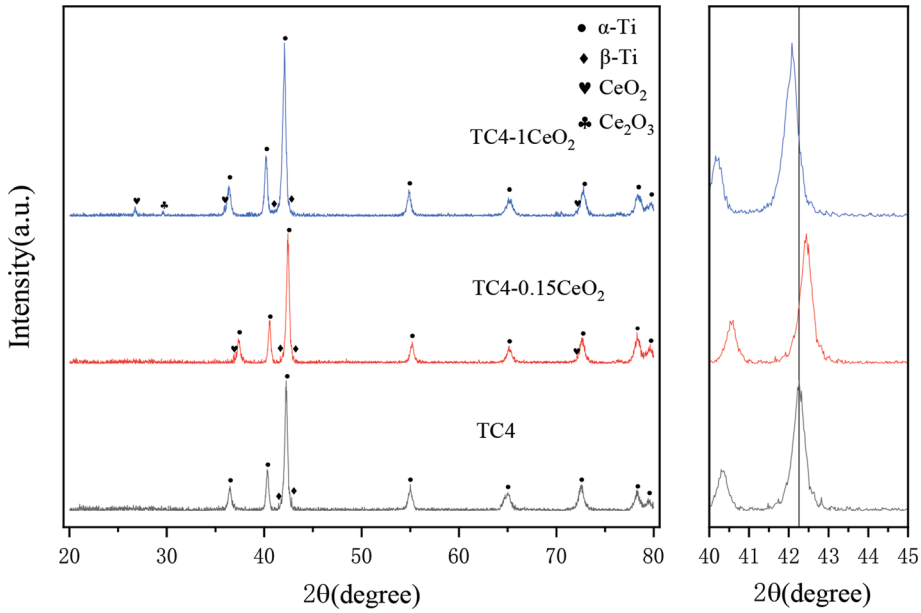

Fig. 5 X-ray diffraction patterns of TC4-xCeO$_2$ alloys

Table 3 Growth restriction factors (Q values) for solutes in the Ti system

Element	m	k	Concentration, Wt Pct	Q*
Al	− 1.7	→ 1	up to 20	→ 0
V	− 2	→ 1	up to 12	→ 0
Fe	− 18	0.82	up to 5	3.2
Ce	− 6.1	0.19	up to 4	4.9

Table 4 Tensile properties of TC4-xCeO$_2$ alloys at room temperature

CeO$_2$ Content, ω%	Yield strength, MPa	Tensile strength, MPa	Elongation, %
0	700	819	8.04%
0.1	1079	1268	4.8%
0.15	1027	1293	5.6%
0.2	1014	1175	3.6%

CeO$_2$ has a higher Gibbs free energy, which increases the temperature of the solidification interface and accelerates the solidification rate, resulting in a more refined alloy structure. Zhang et al. (Ref 37) added CeO$_2$ during laser cladding of titanium-based composite materials and found that CeO$_2$ decomposed into CeO$_2$ and Ce$_2$O$_3$, which they proposed would be pinned at the grain and phase boundaries, thereby hindering grain growth and achieving refinement. In contrast, the characteristic peak of TC4-1CeO$_2$ showed a slight leftward shift in this work, which may have been due to excessive CeO$_2$ addition, which resulted in an increase in lattice constant and interplanar spacing, ultimately leading to coarsening of the alloy structure. This accords with results reported by Wang and Singla (Ref 38, 39), where excessive CeO$_2$ addition resulted in aggregation, decreased crystallographic matching, and ultimately led to coarsening of the alloy structure.

3.3 Mechanical Properties

Figure 6 shows that the microhardness of the TC4 alloy increased with CeO$_2$ content. Based on the microscopic analyses, when the CeO$_2$ content ranged from 0.1 to 0.2%, microhardness was mainly increased by refining the grain size of the alloy structure with CeO$_2$, thereby increasing the density of grain boundaries, and thus increasing resistance-to-dislocation motion during the deformation process. This ultimately resulted in a slight increase in hardness. Considering the CeO$_2$ contents of 0% to 0.1% and 0.2% to 1%, there was a significant increase in microhardness. At these concentrations, grain refinement had little effect: even when the CeO$_2$ content reached 1%, the grains were in a coarsened state. Based on conclusions of other researchers, the increased hardness observed on addition of rare-earth oxides is not only attributed to refinement of the microstructure, but also to reduction in defects, such as cracks and pores (Ref 40, 41). It is possible that the addition of a larger amount of CeO$_2$ enabled the alloy to achieve better formability: at this level of addition, the alloy has already become brittle, therefore resulting in a significant increase in hardness.

Table 4 and Fig. 7 present tensile test results of the TC4-xCeO$_2$ alloy samples. Compared with the original TC4 alloy, addition of a small amount of CeO$_2$ significantly improved the yield strength and tensile strength, but elongation was severely reduced. When the CeO$_2$ content was 0.2%, both the yield strength and tensile strength began to decline, along with a continuous decrease in alloy elongation. When the CeO$_2$ content reached 1%, the sample experienced brittle fracture when separating the TC4 specimen from the forming substrate using an electrical-discharge wire-cutting machine. This increase in brittleness is consistent with the observation that TC4-1CeO$_2$ exhibited the highest hardness value. Based on the above data, addition of CeO$_2$ should not exceed 0.2% and should be controlled below this level.

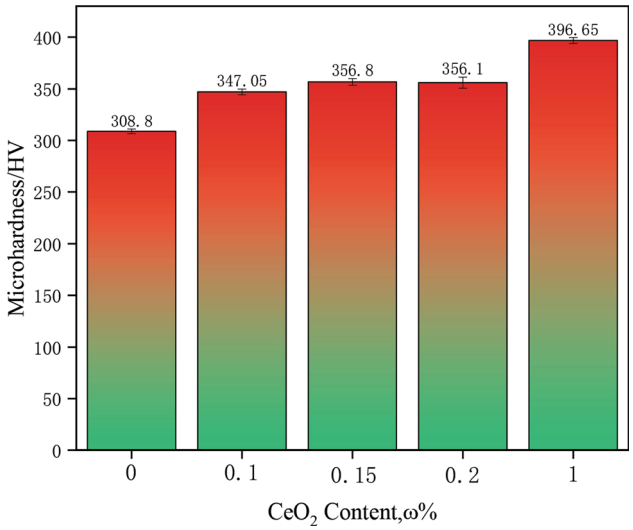

Fig. 6 Hardness histogram of TC4 titanium alloy samples with different CeO_2 contents

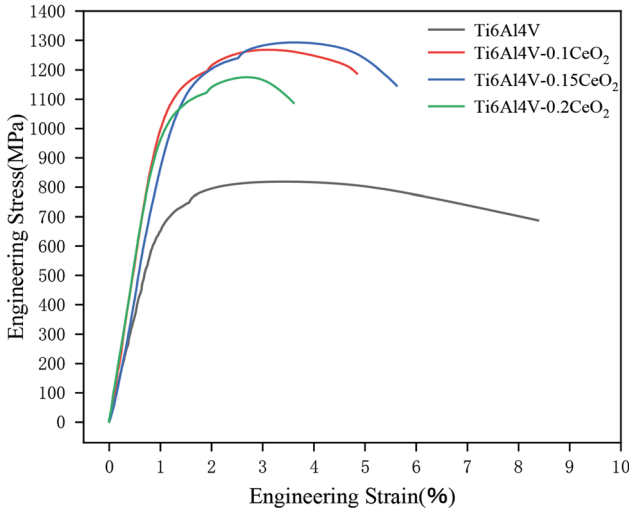

Fig. 7 Engineering tensile stress–strain curves of TC4-$x$$CeO_2$ alloys

Figure 8 shows tensile fracture morphologies of the TC4-$x$$CeO_2$ alloy specimens. The fracture surface of the TC4-0CeO_2 alloy mainly comprised small shallow dimples and indistinct cleavage steps, indicating predominantly ductile fracture. From the enlarged image, it can be observed that the dimples contained some unmelted powder, which is the reason for the lower strength of the TC4-0CeO_2 alloy. The fracture morphologies of the TC4-0.1CeO_2 and TC4-0.15CeO_2 alloys are similar. For these compositions, there was no evidence of unmelted powder in the fracture, the number of dimples decreased compared with the TC4-0CeO_2 alloy, and cleavage steps began to appear. A brittle–ductile mixed fracture mode occurred. With increase in the CeO_2 content, the number of dimples in the fracture of the TC4-0.2CeO_2 alloy significantly decreased, while the number of cleavage steps increased. When the mass fraction of CeO_2 reached 1%, dimples in the fracture surface no longer existed, demonstrating occurrence of a brittle fracture.

Trace amounts of CeO_2 are shown to greatly enhance the strength of the alloy, at the expense of sacrificing a certain degree of plasticity. In addition to the fine-crystal strengthening effect of the rare-earth oxide, CeO_2 can significantly increase absorption of laser radiation on the surface of the metal powder. Li et al. (Ref 42) suggested that adding nano-sized CeO_2 can increase contact between particles and reduce the insulation effect of voids on thermal input, thus increasing thermal conductivity and ultimately improving the laser absorption rate of the cladding layer during laser melting. This greatly improves the challenge of unmelted powder during SLM forming. In addition, CeO_2 can be completely or partially decomposed into Ce and O_2 under high-energy laser irradiation. The former recombines with oxygen in the liquid metal to form CeO_2 and Ce_2O_3. During this process, a certain number of oxygen atoms are eliminated. Research has shown that elimination of oxygen plays an important role in improving plasticity of the alloy, leading to some recovery in the elongation rate of the TC4-0.15CeO_2 alloy. Moreover, as shown in Fig. 1, nano-sized CeO_2 powder can adsorb onto TC4 spherical particles during mixing, which increases its effectiveness; however, when the amount of CeO_2 is too high, both the tensile strength and plasticity of the samples significantly decrease and hardness increases. This may be because excessive addition of rare-earth oxide causes agglomeration, resulting in uneven dispersion and formation of coarse rare-earth oxide particles in the formed parts, which reduces the beneficial effects of this additive (Ref 43, 44). Therefore, there is scope for improvement in the mixing process used in this study: to effectively control the amount of rare-earth oxide and ensure that it is evenly mixed, a planetary ball mill can be used to achieve more thorough mixing of the rare-earth oxide and metal powders.

4. Conclusion

CeO_2 was added at mass fractions of 0.1%, 0.15%, 0.2%, and 1% to TC4 powder, and LSM was used for the formation process to study evolution of the organization and mechanical properties of titanium alloys with different CeO_2 contents. The following conclusions were drawn.

1. CeO_2 has a significant refining effect on the microstructure of SLM-formed TC4. Of the tested alloys, TC4-0.15CeO_2 exhibited the most prominent refining effect, in which the microstructure was transformed from staggered Widmanstätten α plates to mesh-like α plates; however, when the CeO_2 content exceeded 0.2%, the alloy structure started to coarsen.
2. XRD analysis showed that the characteristic peak of TC4-0.15CeO_2 exhibited a slight right shift, indicating that the lattice constants of α and β phases in the alloy were reduced and the grains were refined. Solute-growth inhibition of CeO_2 hindered growth of the originally formed nuclei and CeO_2 entered the titanium lattice interstices, causing lattice distortion and crystal surface shrinkage.
3. Addition of CeO_2 significantly influenced the mechanical properties of SLM-formed TC4. Addition of CeO_2 can increase the hardness of a specimen, but can also damage its plasticity; therefore, the mass fraction of CeO_2 should

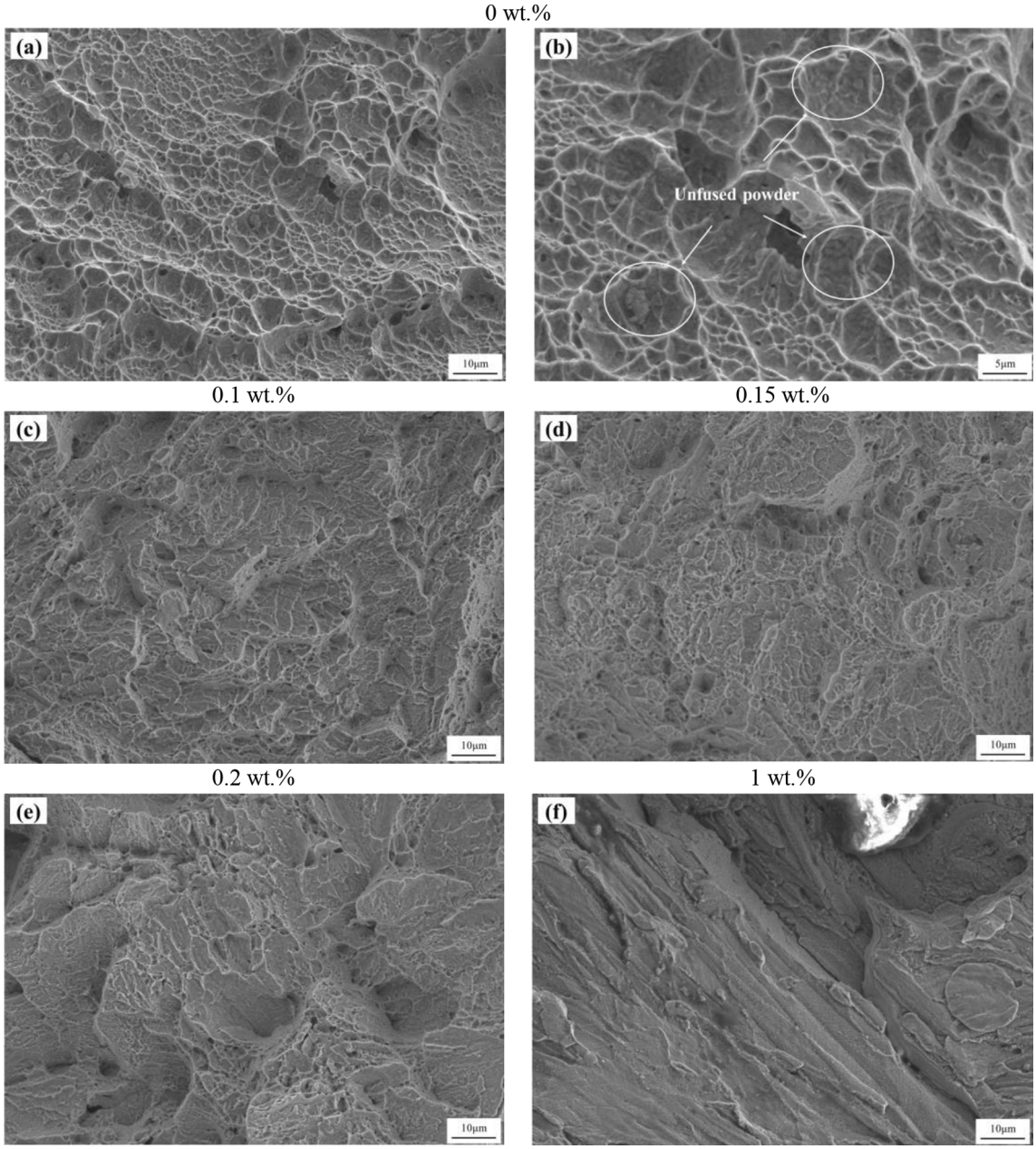

Fig. 8 Fracture morphologies of TC4-xCeO$_2$ alloy specimens: (a) pure TC4; (b) partial enlargement of (a); (c) TC4-0.1CeO$_2$; (d) TC4-0.15CeO$_2$; (e) TC4-0.2CeO$_2$; (f) TC4-1CeO$_2$

be controlled below 0.2%. The yield strength and tensile strength of TC4-0.15 CeO$_2$ alloy reached 1218 and 1293 MPa, respectively, far exceeding the values for the original specimen; its elongation was also the best of the four CeO$_2$ addition levels examined.

Acknowledgments

This work was supported by the National Natural Science Foundation of China (Grant No. 51205359). We thank Kathryn Sole, PhD, from Liwen Bianji (Edanz) (www.liwenbianji.cn) for editing the language of a draft of this manuscript.

Author Contributions

Design was planned by ZHL; experiments were conducted by ZHL, YZ, DDS; data analysis was performed by ZHL, YZ and BY; the manuscript was written by ZHL, YZ; manuscript revision and supervision were conducted by ZHL and BY.

Data and code availability

Not applicable.

Conflict of interest

All authors declare that they have no conflict of interest.

Ethical approval

The authors confirm that the nature of the work did not require prior ethical approval by an institutional review board or equivalent ethics committee.

References

1. J.C. Williams and R.R. Boyer, Opportunities and Issues in the Application of Titanium Alloys for Aerospace Components, *Metals Open Access Metall. J.*, 2020, **10**(6), p 705. https://doi.org/10.3390/met10060705
2. Q. Zhao, Q. Sun, S. Xin, Y. Chen, C. Wu, H. Wang, J. Xu, M. Wan, W. Zeng and Y. Zhao, High-Strength Titanium Alloys for Aerospace Engineering Applications: A Review on Melting-Forging Process, *Mater. Sci. Eng. A Struct. Mater. Prop. Microstruct. Process.*, 2022, **845**, p 143260. https://doi.org/10.1016/j.msea.2022.143260
3. L. Lin, Y. Tian and W. Yu, Corrosion and Hardness Characteristics of Ti/TiN-Modified Ti6Al4V Alloy in Marine Environment, *Ceram. Int.*, 2022, **48**, p 34848–34854. https://doi.org/10.1016/j.ceramint.2022.08.074
4. J. Donoghue, J. Sidhu, A. Wescott and P. Prangnell, Integration of Deformation Processing with Additive Manufacture of Ti-6Al-4V Components for Improved β Grain Structure and Texture, *Springer Int. Publ.*, 2015, **144**, p 437–444. https://doi.org/10.1007/978-3-319-48127-2_55
5. Y.M. Ren, X. Lin, X. Fu, H. Tan, J. Chen and W.D. Huang, Microstructure and Deformation Behavior of Ti-6Al-4V Alloy by High-Power Laser Solid Forming, *Acta Mater.*, 2017, **132**, p 82–95. https://doi.org/10.1016/j.actamat.2017.04.026
6. S. Campanelli, G. Casalino, N. Contuzzi, A. Angelastro, A.D. Ludovico, Analysis of the molten/solidified zone in selective laser melted parts, in *SPIE LASE. International Society for Optics and Photonics*, 2014, https://doi.org/10.1117/12.2042170
7. J.P. Kruth, G. Levy, F. Klocke and T.H.C. Childs, Consolidation Phenomena in Laser and Powder-Bed Based Layered Manufacturing, *CIRP Ann. Manuf. Technol.*, 2007, **56**(2), p 730–759. https://doi.org/10.1016/j.cirp.2007.10.004
8. M. Simonelli, N.T. Aboulkhair, P. Cohen, J.W. Murray, A.T. Clare, C. Tuck and R.J.M. Hague, A comparison of Ti-6Al-4V In-Situ Alloying in Selective Laser Melting Using Simply-Mixed and Satellited Powder Blend Feedstocks, *Mater Charact*, 2018, **143**, p 118–126. https://doi.org/10.1016/j.matchar.2018.05.039
9. A.K. Singla, M. Banerjee, A. Sharma, J. Singh and D.K. Goyal, Selective Laser Melting of Ti6Al4V Alloy: Process Parameters, Defects and Post-Treatments, *J. Manuf. Process.*, 2021, **64**, p 161–187. https://doi.org/10.1016/j.jmapro.2021.01.009
10. N. Sanaei and A. Fatemi, Defects in Additive Manufactured Metals and Their Effect on Fatigue Performance: A State-of-the-Art Review, *Prog. Mater. Sci.*, 2020, **117**, p 100724. https://doi.org/10.1016/j.pmatsci.2020.100724
11. H. Ali, H. Ghadbeigi and K. Mumtaz, Effect of Scanning Strategies on Residual Stress and Mechanical Properties of Selective Laser Melted Ti6Al4V, *Mater. Sci. Eng. A*, 2018, **712**, p 175–187. https://doi.org/10.1016/j.msea.2017.11.103
12. H. Li, X. Liu, Y. Li, S. Zhang, Y. Chen, S. Wang, J. Liu and J. Wu, Effects of Rare Earth Ce Addition on Microstructure and Mechanical Properties of Impure Copper Containing Pb, *Trans. Nonferrous Metals Soc. China*, 2020, **30**(6), p 1574–1581. https://doi.org/10.1016/S1003-6326(20)65320-1
13. M.J. Bermingham, S.D. McDonald and M.S. Dargusch, Effect of Trace Lanthanum Hexaboride and Boron Additions on Microstructure, Tensile Properties and Anisotropy of Ti-6Al-4V Produced by Additive Manufacturing, *Mater. Sci. Eng. A*, 2018, **719**, p 1–11. https://doi.org/10.1016/j.msea.2018.02.012
14. Y.F. Yang, S.D. Luo, G.B. Schaffer and M. Qian, Impurity Scavenging, Microstructural Refinement and Mechanical Properties of Powder Metallurgy Titanium and Titanium Alloys by a Small Addition of Cerium Silicide, *Mater. Sci. Eng. A Struct. Mater. Prop. Microstruct. Process.*, 2013, **573**(Jun 20), p 166–174. https://doi.org/10.1016/j.msea.2013.02.042
15. K.M. Li, Y.J. Liu, X.C. Liu, X. Wu, S.F. Zhou, L.C. Zhang, W. Li and W.C. Zhang, Simultaneous Strength-Ductility Enhancement in as-cast Ti6Al4V Alloy by Trace Ce, *Mater. Des.*, 2022, **215**, p 110491. https://doi.org/10.1016/j.matdes.2022.110491
16. Y. Xu, Z. Liu, X. Zhu, Z. Jiang, H. Chen and N. Wang, Effect of Rare Earth Ce Addition on Microstructure and Mechanical Properties of Titanium Alloy Ti-6Al-4V, *Mater. Lett.*, 2023, **330**, p 133244. https://doi.org/10.1016/j.matlet.2022.133244
17. C. Wang, Y. Gao, Z. Zeng and Y. Fu, Effect of Rare-Earth on Friction and Wear Properties of Laser Cladding Ni-Based Coatings on 6063Al, *J. Alloys Compd.*, 2017, **727**, p 278–285. https://doi.org/10.1016/j.jallcom.2017.08.101
18. S.M. Sastry, P.J. Meschter and J.E. Oneal, Structure and Properties of Rapidly Solidified Dispersion-Strengthened Titanium Alloys: Part I. Characterization of Dispersoid Distribution, Structure, and Chemistry, *Metall. Mater. Trans. A*, 1984, **15**(7), p 1451–1463. https://doi.org/10.1007/BF02648575
19. D.S. Schwartz, P. Fraundorf and S.M.L. Sastry, TEM study of B- and Er-Containing Dispersoids in Rapidly Solidified Dispersion-Strengthened Titanium and Titanium Aluminide Alloys, *Ultramicroscopy*, 1991, **37**(1–4), p 310–317. https://doi.org/10.1016/0304-3991(91)90028-5
20. S.A. Court, J.W. Sears, M.H. Loretto and H.L. Fraser, The Effect of Liquid Phase Separation on the Microstructure of Rapidly Solidified Titanium−Rare Earth Alloys, *Mater. Sci. Eng. A*, 1988, **98**, p 243–249. https://doi.org/10.1016/0025-5416(88)90163-2
21. Z. Wang, Z. Xiao, Y. Tse, C. Huang and W. Zhang, Optimization of Processing Parameters and Establishment of a Relationship Between Microstructure and Mechanical Properties of SLM Titanium Alloy, *Opt. Laser Technol.*, 2019, **112**, p 159–167. https://doi.org/10.1016/j.optlastec.2018.11.014
22. D. Sun, D. Gu, K. Lin, J. Ma, W. Chen, J. Huang, X. Sun and M. Chu, Selective Laser Melting of Titanium Parts: Influence of Laser Process Parameters on Macro- and Microstructures and Tensile Property, *Powder Technol. Int. J. Sci. Technol. Wet Dry Part. Syst.*, 2019, **342**, p 371–379. https://doi.org/10.1016/j.powtec.2018.09.090
23. F. Zhang, J. Chen, H. Tan, X. Lin and W. Huang, Effects of Rare Earth Nd on Microstructure and Mechanical Properties of Laser Rapid Formed TC4 Titanium Alloy, *Rare Metal. Mater. Eng.*, 2007, **36**(8), p 5.
24. F.R. Kaschel, M. Celikin and D.P. Dowling, Effects of Laser Power on Geometry, Microstructure and Mechanical Properties of Printed Ti-6Al-4V Parts, *J. Mater. Process. Technol.*, 2019, **278**, p 116539. https://doi.org/10.1016/j.jmatprotec.2019.116539
25. J. Yang, J. Han, H. Yu, J. Yin, M. Gao, Z. Wang and X. Zeng, Role of Molten Pool Mode on Formability, Microstructure and Mechanical Properties of Selective Laser Melted Ti-6Al-4V Alloy, *Mater. Des.*, 2016, **110**, p 558–570. https://doi.org/10.1016/j.matdes.2016.08.036
26. Y. Liu, R. Sun, N. Wei, T. Zhang and Y. Lei, Effects of CeO_2 on Microstructure and Properties of TiC/Ti_2Ni Reinforced Ti-Based Laser Cladding Composite Coatings, *Opt. Lasers Eng.*, 2019, **120**, p 84–94. https://doi.org/10.1016/j.optlaseng.2019.03.001
27. Q. Fan, A New Method of Calculating Interplanar Spacing: The Position-Factor Method, *J. Appl. Crystallogr.*, 2012, **45**(6), p 1303–1308. https://doi.org/10.1107/S0021889812037764
28. C.G. Pope, X-ray Diffraction and the Bragg Equation, *J.Chem. Edu.*, 1997, **74**(1), p 129–131. https://doi.org/10.1021/ed074p129
29. W. Yan, H. Wang, H. Tang, X. Cheng and Y. Zhu, Effect of Nd Addition on Microstructure and Tensile Properties of Laser Additive Manufactured TC11 Titanium Alloy, *Trans. Nonferrous Metals Soc. China*, 2022, **32**(5), p 1501–1512. https://doi.org/10.1016/S1003-6326(22)65889-8
30. I. Maxwell and A. Hellawell, A Simple Model for Grain Refinement during Solidification, *Acta Metall.*, 1975, **23**(2), p 229–237. https://doi.org/10.1016/0001-6160(75)90188-1
31. L. Yiming, J. Yunping, K. Xueliang and R. Huiping, Research Progress of Effects of Rare Earth Elements on Metal Additive Manufacturing, *Rare Metal Mater. Eng.*, 2022, **51**(9), p 14.
32. M.A. Easton and D.H. StJohn, A Model of Grain Refinement Incorporating Alloy Constitution and Potency of Heterogeneous Nucleant Particles, *Acta Mater.*, 2001, **49**(10), p 1867–1878. https://doi.org/10.1016/S1359-6454(00)00368-2
33. D. Zhang, D. Qiu, M.A. Gibson, Y. Zheng, H.L. Fraser, D.H. StJohn and M.A. Easton, Additive Manufacturing of Ultrafine-Grained High-Strength Titanium Alloys, *Nature*, 2019, **576**(7785), p 91–95.

34. Q. Zhenjia, Z. Xiaoxing, W. Yuyue, H. Hao and Z. Anfenget, Effect of B on Microstructure and Tensile Properties of Laser Additive Manufactured TC4 Alloy, *Chin. J. Lasers*, 2020, **47**(6), p 0602002. https://doi.org/10.3788/CJL202047.0602002
35. D. Zhang, A. Prasad, M.J. Bermingham, C.J. Todaro, M.J. Benoit, M.N. Patel, D. Qiu, D.H. StJohn, M. Qian and M.A. Easton, Grain Refinement of Alloys in Fusion-Based Additive Manufacturing Processes, *Metall. and Mater. Trans. A.*, 2020, **51**, p 4341–4359. https://doi.org/10.1007/s11661-020-05880-4
36. S. Zhang, M. Li, J. Yoon, T. Cho, C. Lee and Y. He, The Comparative Study on Microstructure and Properties of Nano-CeO_2 and Sm_2O_3 Particulate Reinforced Nickel-Based Composites by Laser Deposition, *Appl. Surf. Sci.*, 2008, **254**(22), p 7446–7452. https://doi.org/10.1016/j.apsusc.2008.06.011
37. Z. Zhang, F. Yang, H. Zhang, T. Zhang, H. Wang, Y. Xu and Q. Ma, Influence of CeO_2 Addition on Forming Quality and Microstructure of TiC-Reinforced CrTi4-Based Laser Cladding Composite Coating, *Mater Charact*, 2020, **171**(Part 2), p 110732. https://doi.org/10.1016/j.matchar.2020.110732
38. K. Wang, Q. Zhang, M. Sun and X. Wei, Microstructural Characteristics of Laser Clad Coatings with Rare Earth Metal Elements, *J. Mater. Process. Technol.*, 2003, **139**, p 448–452. https://doi.org/10.1016/S0924-0136(03)00551-X
39. Y. Singla, N. Arora and D.K. Dwivedi, Dry Sliding Adhesive Wear Characteristics of Fe-Based Hardfacing Alloys with Different CeO_2 Additives—A Statistical Analysis, *Tribol. Int.*, 2017, **105**(Completed), p 229–240. https://doi.org/10.1016/j.triboint.2016.10.015
40. G. Zhang, C. Wang, Y. Gao, W. Wei and X. Lu, Microstructure and Wear Resistance of CeO_2+Ni60A Composite Coating on Aluminum Alloys by Laser Cladding, *Rare Metal Mater. Eng.*, 2015, **44**(5), p 1229–1233. https://www.rmme.ac.cn/rmmeen/article/abstract/20150539
41. L. Jun, H. Wang, L. Manping and Y. Zhishui, Effect of Yttrium on Microstructure and Mechanical Properties of Laser clad Coatings Reinforced by In Situ Synthesized TiB and TiC, *J. Rare Earths*, 2011, **29**(5), p 477–483. https://doi.org/10.1016/S1002-0721(10)60483-8
42. M. Li, S. Zhang, H. Li, Y. He, J. Yoon and T. Cho, Effect of Nano-CeO_2 on Cobalt-Based Alloy Laser Coatings, *J. Mater. Process. Tech.*, 2008, **202**(1–3), p 107–111. https://doi.org/10.1016/j.jmatprotec.2007.08.050
43. L. Ding and S. Hu, Effect of Nano-CeO_2 on Microstructure and Wear Resistance of Co-Based Coatings, *Surf. Coat. Technol.*, 2015, **276**, p 565–572. https://doi.org/10.1016/j.surfcoat.2015.06.014
44. R. Savinov, Y. Wang and J. Shi, Microstructure and Properties of CeO_2-Doped CoCrFeMnNi High Entropy Alloy Fabricated by Laser Metal Deposition, *J. Manuf. Process.*, 2020, **56**, p 1245–1251. https://doi.org/10.1016/j.jmapro.2020.04.018